

# Health monitoring of composite materials based on BP sensors under complex environments

Xiaoqiang Wang<sup>1</sup>, Hailong Tang<sup>1</sup>, Shaowei Lu<sup>2</sup> ✉, Junchi Ma<sup>2</sup>, Keming Ma<sup>2</sup>, Shuai Wang<sup>1</sup>, Xiangdong Yang<sup>2</sup>

<sup>1</sup>Faculty of Aeronautical and Astronautical Engineering, Shenyang Aerospace University (SAU), Shenyang, 110136, People's Republic of China

<sup>2</sup>Faculty of Materials Science and Engineering, Shenyang Aerospace University (SAU), Shenyang, 110136, People's Republic of China

✉ E-mail: lushaowei\_2005@163.com

Published in Micro & Nano Letters; Received on 11th May 2019; Revised on 14th September 2019; Accepted on 21st October 2019

In this study, the air thermal cycle test and the relative humidity (RH) cycle test were carried out to buckypaper (BP) co-cured with glass fibre prepreg together in order to verify the practicality and stability of the sensor in complex environment. The BP bonded with composite laminate were subjected to tension and tension–tension fatigue up to 1000 cycles when the sensor is subjected to temperature changed from 20 to 120°C and different RH from 0 to 85%, respectively, and the electrical–mechanical response shows that the resistance of sensor increases as the humidity increases, and ultimately the change rate tends to be stable. Tensile experiments shows that gauge factor (GF) changes by 327 and 306%, respectively. The authors finished the fatigue experiment to specimen of the longest environmental treatment in order to further verify the practicality of the sensors, in the fatigue test, the resistance change rate varies with the number of cycles, and it tends to be stable after a period of time. The authors draw the curve of GF and fatigue cycle number so that the stability of the sensors are better reflected, the result is consistent with the fatigue result. Therefore, BP sensors can be applied to the health monitoring of aerospace composites.

**1. Introduction:** Over the past several years, glass fibre reinforced have emerged in a wide range of primary structural applications, these structures, such as aircraft fuselage and wings, undergo complex thermal and moisture during their service life. In order to extend the usage of such materials, the reliability of structure has to be ensured in a safe, simple and economical manner. Structural health monitoring (SHM) has become increasingly important to improve the safety and reliability of these advanced composite structures. At present, commonly health monitoring methods are mainly non-destructive testing and sensors testing. Non-destructive monitoring technology cannot serve for large-scale application because of the unpredictability of damage and the difficulty of dismantling large components. Conventional metallic strain manufactured by Simmons and Ruge is not a good choice owing to the single direction. FBG with high sensitivity and multiplexing capabilities over traditional sensors have widely been used in polymer composites for strain monitoring and damage detection, however, its disadvantages such as high price and fragility limit its application. The appearance of carbon nanotubes (CNTs) by Iijima [1] has attracted remarkable attention owing to their remarkable thermal and electrical conductivities, superior mechanical properties and low density [2]. Now, CNTs have been used to modify the polymer matrix of conventional continuous fibre reinforced polymer composites. Wang *et al.* [3] fabricated CNT-reinforced buckypapers (BPs) by dispersing CNTs into water with the aid of epoxy resin. The storage moduli of these nanocomposites were 429% higher compared to neat resin modulus. Thostenson and Chou [4] demonstrated the damage sensing capability of CNTs manufacturing sensors around structural fibre reinforcement where conductive networks in the polymer matrix was achieved by dispersing nanotubes in epoxy and then infusing into glass fibre preforms, it showed that the networks were highly sensitive to strain as well as the onset of matrix-dominated failure mechanisms. Kunkun *et al.* [5] made a flexible and highly sensitive temperature sensor using CNTs and rubber. The results show that the temperature sensor has high linearity, good repeatability and high negative temperature coefficient of resistance

(NTC = −54.7/°C). Wichman *et al.* [6] also noticed that the thermal convection positively influences the CNT network formation in CNT-doped resin composites. Yin *et al.* [7] performed the dynamic strain response of MWCNTs/epoxy nanocomposites with different aspect ratios and dispersion states. Cao *et al.* [8] investigated the humidity-sensitive properties of MWCNTs systematically and proposed that the sensitivity of CNTs to humidity can be enhanced with chemical treatment, it showed that CNTs usually generate inhomogeneous dispersions and large aggregates because of the Van der Waals interactions [9]. A common characteristic of the above fillers is that they need to be dispersed into the material, which makes them difficult for a wide variety of applications because of their aggregation. In fact, the sensors prepared may be different from the ones expected since it is not possible to avoid aggregates because of a not uniform dispersion of fillers within the resin. The conductive network inside the sensor may be missing, and thereby affect the sensitivity and stability of the sensor.

Thus, there have been advances in producing CNTs, such as films referred to as BP [10], BP is an outstanding material which contains entangled networks of CNTs formed by van der Waals interactions, and fabricated by using SWCNTs [11], double-walled CNTs [12], and MWCNTs [13]. Koratkar *et al.* [14, 15] fabricated BP by using catalytic chemical vapour deposition of xylene–ferrocene mixture precursor. Slobodian *et al.* [16] integrate the BP embedded in a polyurethane membrane into a glass fibre reinforced epoxy composite by means of a vacuum infusion. Wang *et al.* [17] have fabricated highly oriented BP made of aligned CNTs. Comparison of BP and conventional CNT dispersions, BP sensors are more favourable than CNTs/polymer nanocomposites, it may be reunited since low solubility and weak dispersibility of CNTs within the polymer matrix. Aly and Bradford [18] embedded BP sensors into composites to monitor the response of sensors after impact at different positions of composites in real time. Gou *et al.* [19] used BP as both interlayer and surface layer of the laminates to enhance the damping properties. The damping testing on the nanocomposite

beam indicated up to 200–700% compared to traditional composite beam. The BP can be bonded with composite laminates in high-performance aerospace composites, and the ability of the polymer matrix to infiltrate the BP sensors in addition to the CNT film-matrix interaction is important that change the sensing behaviour of the nanotube film. The CNT network and matrix interaction during processing was extensively analysed by Luo *et al.* [20, 21], it showed that CNTs are promising candidates for multi-purpose sensing approaches considering both manufacturing process and mechanical behaviour of composite. Wang *et al.* [22] investigated the mechanical properties of BP integrated carbon-fibre composites under tensile loading. Sinan *et al.* [23] discuss the real-time sensing behaviour of BP sensors interleaved between cross-ply carbon fibre-epoxy laminate under uniaxial fatigue loading conditions. During the lifetime of sensor, environmental effects such as humidity and temperature affect the conduction properties and functionality of the sensor. It is very significant to certify the stable of BP sensors under high relative humidity (RH). Koratkar *et al.* [24] studied the electronic transport of BP between – 150 and 300°C. It was found that the temperature sensitivity of BP was independent of heating/cooling rate and without hysteresis. Li *et al.* [25] used graphene oxide and multi-walled CNTs to prepare high sensitivity humidity sensors. The results show that the sensitivity of the sensor is 13 times that of graphene oxide. Bi *et al.* [26] developed a capacitive humidity sensor using GO as a sensing material. The desired sensing effect cannot be achieved because the interaction of GO with water molecules produces some change in the electrical impedance of GO film. Trulli *et al.* [27] evaluated the physical-chemical properties and the colloidal stability of the plasma-treated MWCNTs. Bradley *et al.* developed CNTs based field-effect transistors for humidity monitoring [28]. Memon *et al.* [29] explored the thermal impedance of carbon nanofibre (CNF)-based BP with a heat treatment temperatures of 1100, 1500 and 3000°C. Other studies reported the resistance temperature response in pristine MWCNT films in the temperature range of – 195–20°C [30] and 20–200°C [31]. Yoo *et al.* [32] proposed a resistive-type humidity sensor based on plasma-treated MWCNTs/polyimide composite films, but the sensitivity was just 0.0047/% RH. In spite of some studies aimed at research the strain sensing properties of composite reinforced with carbon-based nanofillers, some critical issues still have to be expounded in order to fully make use of their advantageous characteristics. Most studies have just focused on the ordinary electrical/mechanical sensing behaviour. Comparatively few studies focused on the ability of sensor bonded with fibre-reinforced composites with simulated real-world application environment.

In this study, one rectangular BP sensor fabricated by spray-vacuum monodisperse MWCNTs was bonded to the composite laminate. Placing the sample in a closed chamber to better match the actual environment. The resistance of the BP sensor was monitored in real time using a Fluke instrument, and then the fatigue and tensile tests were performed at room temperature using a universal testing machine, and the changes of resistance ( $\Delta R/R_0$ ) and strain ( $\epsilon$ ) and the residual resistance change with fatigue times are discussed.

## 2. Experimental set-up

2.1. Fabrication of BP: In this paper, MWCNTs (diameter: 8–15 nm, length: 50  $\mu$ m, purity: 98%) were provided by Chengdu

Organic Chemicals Pty Ltd, the Chinese Academy of Sciences. Before this procedure, a parametric study was performed to optimise the preparation procedure of MWCNTs' dispersion. The process parameter ranges and their optimum values, including MWCNTs concentration, MWCNTs-to-surfactant ratio, sonication time and powder, are presented in Table 1. The preparation process of BP was as follows: 600 mg MWCNTs and 5 ml Triton X-100 were added in 200 ml deionised water to obtain MWCNTs aqueous solution. The MWCNTs solution was sonicated three times (each time 20 min) at 100 W and then centrifuged for 40 min at 6000 r/min. The sonicator (Q700, Sonicator Co., Ltd, USA) was operated in a pulse mode (on 2 s, off 2 s). On completion of the dispersion process, the MWCNTs mono-dispersion solution was ejected onto a 0.45  $\mu$ m porous diameter filter membrane and filtered by a spray-vacuum filtration setup. After that, the filter paper was left in a fan oven and dried at 80°C for 8 h and peeled off as shown in Fig. 1a.

2.2. Fabrication of the glass fibre composite laminates surface bonded with BP: In this section, the glass/epoxy unidirectional prepreg (model CFB-17500; Dezhou Carbon Fiber Composites Co. Ltd, China) was used attributed to its extremely high mechanical, good heat resistance, strong adhesion with the nanocomposites and dielectric properties, the geometric size of material is 250  $\times$  250 mm. The fabricated BP was cut into a rectangular strip (30  $\times$  10 mm) as shown in Fig. 2 and then they were put onto the composite laminates. Then the laminates were cured at 120°C for 2.5 h with a pressure of 2 MPa by the moulding machine (Dongguan YiTong Test & Technology Co. Ltd, China), and then they were cooled to room temperature with constant pressure. The manufacturing process of the glass fibre composite laminates and the position of sensors were shown in Fig. 2.

2.3. Measurement: The micro morphologies of the BP and BP bonded with the composite laminates were studied by scanning electron microscopy (S-4800, Hitachi, Japan). The samples are placed into programmable constant temperature and humidity test chamber (LRHS-225-LH, China, temperature range from 0 to 150°C, humidity range 0–100%). In the air thermal cycle (ATC), one thermal cycle was defined as a change from 20 to 120°C, and finally back to 20°C. The heating rate of the instrument was 3°C/min and the dwell times at 120°C were set to 30 min to reach thermal equilibrium. For the RH, the humidity were 0, 20, 40, 60 and 85%, for each RH, the corresponding temperature and time for environmental treatment of the sensor are 80°C and 100 h, respectively. The composite laminates bonded with BP sensors were cut from the material plates according to the ASTM D3039. To evaluate the sensing performance of the BP sensor after the processing of ATC or RH, different modes of tensile loading were performed using INSTRON-8801 test system (Fig. 3) in a controlled laboratory environment. These tests included: (i) monotonic tensile tests with a fixed displacement speed of 2 mm/min, and (ii) fatigue tensile tests with frequency of 0.5 Hz for 1000 cycles, during each fatigue tests, the specimens were tested with a maximum strain of 0.12%. The force data was recorded by the testing machine load cell while the strain was recorded via the metal foil strain gauge. The electrical resistance of the BP sensor was recorded by FLUKE 2638 A multimeter.

**Table 1** Process parameters for the preparation of MWCNTs dispersions

Material	MWCNTs concentration, mg/ml	MWCNTs-to- TX-100 ration	MWCNTS sonication time, min/power, W	Centrifugal time, min/force, $\times 10^3$ g
range	0.5–5	1:1–1:12	3–45/30–180	15–60/2–10
optimal value	3	1:8	60/100	40/8

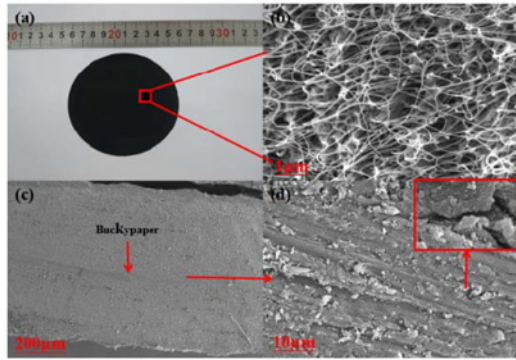


**Fig. 1** Scanning Electron Microscope (SEM)  
a Original view of BP,  
b SEM of the BP,  
c, d SEM of BP co-cured with the composite

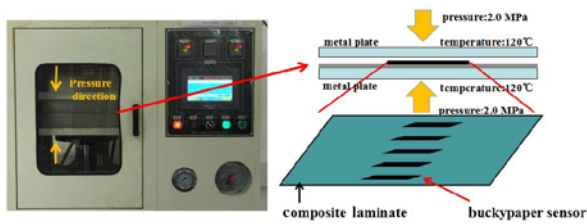


**Fig. 2** Schematic diagram of fabrication of composite laminates

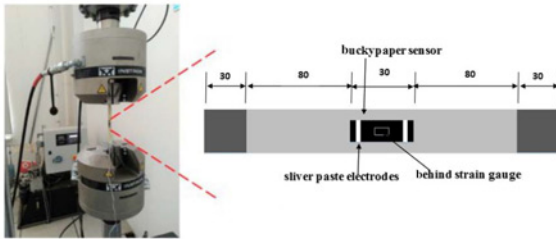


**Fig. 3** Experimental setup and specimen characteristics for BP sensor's characterisation in tensile tests

It is essential to point out that both the strain gauge data acquisition software and the multimeter program were started simultaneously to guarantee precise correlation of strain and resistance data. And at least three samples were selected to evaluate the electromechanical responses in order to avoid the contingency of the result.

### 3. Results and discussion

**3.1. Microstructure analysis of BP:** The original view and the scanning electron microscopy (SEM) images of the pristine BP are shown in Figs. 1a and b, there are many connections formed by a complete conductive path to each other between CNTs since the CNTs naturally tend to be in a bent state, this feature can be verified from Fig. 1b, the internal pores of BP are uniform, and there is no obvious phenomenon of CNT agglomeration, which facilitates the wetting of the resin so that the strain change of the specimen can be accurately detected. In Fig. 1b, we can conclude that BP is a unique three-dimensional structure intertwined by CNTs, the unique structure of BP contributes the transfer of charge to facilitate the formation of high conductivity, which lays a good structural basis for the practical application of BP. Figs. 1c and d show a cross-sectional view of BP co-cured with composites. In Fig. 1c, there is no delamination between BP and

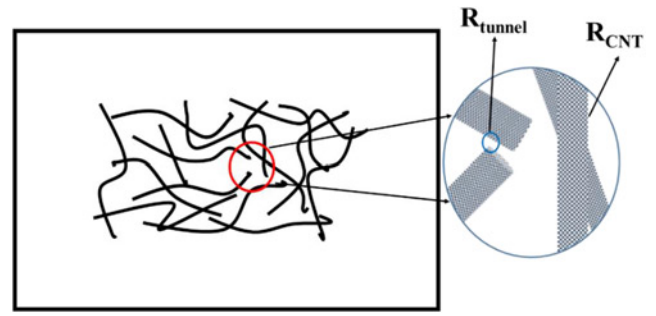


**Fig. 4** Conductive microstructure diagram of BP

specimen, and BP can be deformed together with the specimen which prove the accuracy of the correspondence between resistance and strain in the tensile result. As can be seen from Fig. 1d, the resin has been completely immersed the BP sensor, the resistance of BP can reflect accurately real-time strain of specimen.

**3.2. BP sensors sensing mechanism:** It is crucial to investigate the structures of the BP sensors in order to better understand the mechanism of the experiment. The microstructure of BP is shown in Fig. 4. The change in resistance of BP sensors with applied strain relies mainly on the changes of conduction networks, including the tunnelling effect originating from the change in distance between two adjacent nanofillers, and the existing inherent resistance of nanoscale fillers such as CNTs. The contact resistance plays a dominant role in the electrical conductivity of BP sensor, the average distance between two adjacent nanoparticles alters under externally applied strain, which leading to the tunnelling of charged carriers and a consequent increase in local electrical conductivity. In the actual application process, we have introduced the concept of gauge factor (GF) in order to better reflect the sensitivity and stability of the sensor, the GF which relates the resistance change ( $\Delta R/R_0$ ) to the axial strain ( $\epsilon$ ) is evaluated as  $GF = \Delta R/R_0$  where  $R_0$  is the initial resistance of BP sensors at the beginning of the experiment, and  $\Delta R = R - R_0$  is the resistance variation. Strain ( $\epsilon$ ), which is used to evaluate the relative change of the strain gauge was recorded by DH3821 Digital Signal Collector.

**3.3. Tensile and fatigue of the samples after ATC:** For different ATCs, the strain ( $\epsilon$ ) and the change in electrical resistivity ( $\Delta R/R_0$ ) of the BP sensor were platted as a function as shown in Fig. 5. There were four different ATCs (from 20°C to 120°C) for

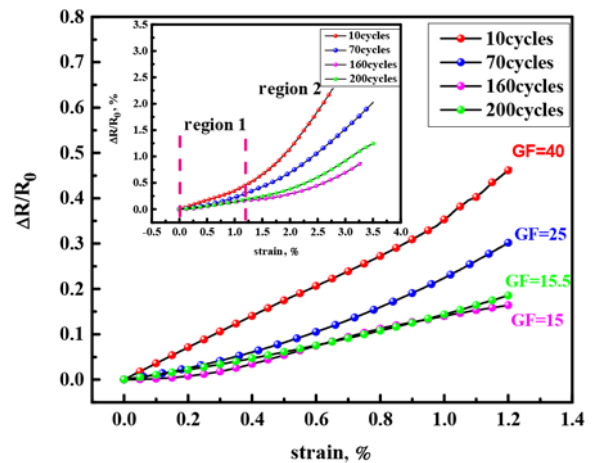


**Fig. 5** Relative resistance changes as a function of strain for BP sensor bonded with composite laminates for different ATCs



10 cycles, 70 cycles, 160 cycles and 200 cycles. For region 1 (strain from 0 to 1.2%), the rate of change in resistance increased linearly with strain for different ATCs. It can be seen in Fig. 5, the GF of BP sensor decreased as the ATCs increased. The thermal expansion coefficient of the resin, fibre and the CNTs was different when the sample was subjected to the temperature cycles, there would be a relatively large expansion for resin. Then the molecules of the resin matrix would crosslink with each other and there would appear the separation of resin from the interface. In the tensile test, compared with the composite laminates there would be a relatively small deformation for resin. The conductivity network of the BP sensor which was infiltrated with resin was destroyed more slowly. So that, for the same strain for the samples by different ATCs, the rate of change in resistance were smaller after the more ATCs. The GF of the 160 cycles and 200 cycles were almost the same. The reason was that when the ATCs reached the 160 cycles, the sample tended to stabilise and the influence from the thermal cycle can be ignored. However, in region 2 (strain from 0 to 3.5%), there was a little difference between the 160 cycles and 200 cycles. The GF of the 200-cycles was a little larger than 160-cycles, the reason is that after the 200 cycles the substrate appeared tiny rupture. In short, the sensor after the ATCs of 200 was stable and sensitive for the strain from 0 to 1.2%.

The specimen was carried out 1000 cyclic fatigue tests to verify that BP sensors possess the long-term durability in a similar practical environment. During the fatigue experiment process, we reduced the sampling frequency to gain the detailed data of 1–10, 100–110, 500–510 and 990–1000 cycles, so that to better observe the corresponding relationship between sensor resistance and strain, Fig. 6a shows the electrical response of the BP sensor undergoing cyclic fatigue loading, detailed data information collected by slowing down frequency are shown in Figs. 6b–e, respectively.  $\Delta R/R_0$  shows a rising trend at an early stage from the overall fatigue results, it can be explained that residual resistance is generated during each cycle, thus the initial resistance of each cycle does not reach the original position. In the strain-resistance change rate-time curve of Fig. 6b, the resistance change rate and time have very good linearity during the load-unload process, and strain-time has a very good consistency and synchronism. The resistance change rate closely follows the increase of strain as time increases and shows obvious linear relationship which corresponds to the resistance change caused by micro-strain in tensile tests. In the 100–110 cycles experiment, the resistance rate is roughly stabilised

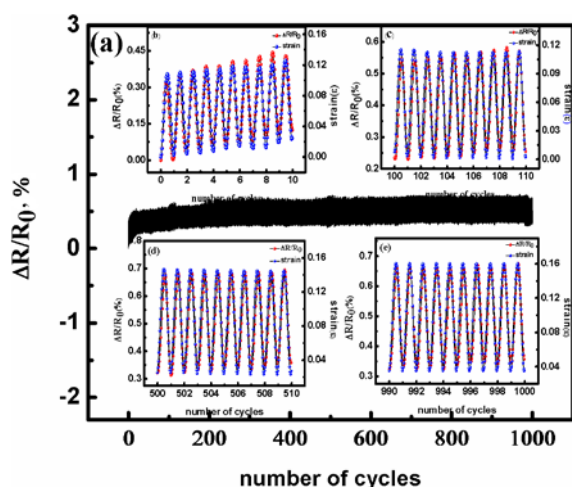


**Fig. 6** Real-time electrical and mechanical response under cyclic fatigue loading of the BP sensors  
a Real-time electrical and mechanical response under cyclic fatigue loading of the BP sensors, and  
b–e The 10, 100, 500, 1000 cycles

at around 0.55%, which indicated that the residual resistance has been stable. During the 500–510 cycles, the resistance change rate is stable at 0.68%, which is higher than the previous results. the reason may be that the local damage caused by the composite materials because of environmental treatment, which makes the composite materials produced greater strain under the same tensile force so that the BP generates corresponding resistance response. This phenomenon also reflects the superiority of BP in health monitoring. Therefore, the excellent durability of BP sensors warrants their application as sensing elements for SHM of high-performance polymeric composite.

In order to further validate the previous experimental results, the variation of the GF with the number of cycles, residual resistivity and cycle number were analysed, as shown in Fig. 7a, GF upon loading and unloading showed significant changes in the initial cycles, which were similar to changes in fatigue experiments. During the subsequent loading and unloading process, the change of GF gradually stabilised in 0.3%. GF upon loading and unloading are similar in each cycle, it may be deduced from this result that the sensor maintains reversibility and stability. The residual resistivity of the sensor appears to accumulate in the early stage due to the damage of the internal structure. The residual resistance tends to be stable after a certain period of tension–tension fatigue as shown in Fig. 7b. Therefore, the sensors can be used for material health monitoring in special environments.

3.4. Tensile and fatigue of the samples after RH: Three samples experiments were designed in order to illustrate the effect of humidity for the BP sensors. The relative resistance change of the BP sensors was measured with the resistance collector under different humidity, responsively. Fig. 8 displayed that the resistance change of BP sensor increased sharply first, and the relative change of the resistance gradually stabilised as the environmental

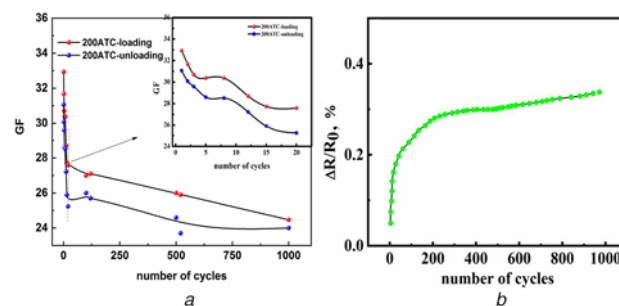


**Fig. 7** Curve of GF and residual resistance after air thermal cycle  
a GF and corresponding cycle  
b Residual resistivity change with cycle numbers

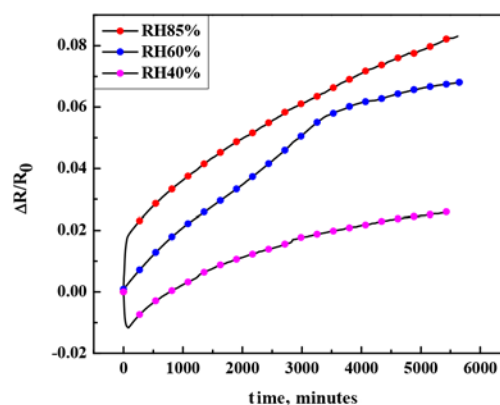


**Fig. 8** Resistance-RH response of BP

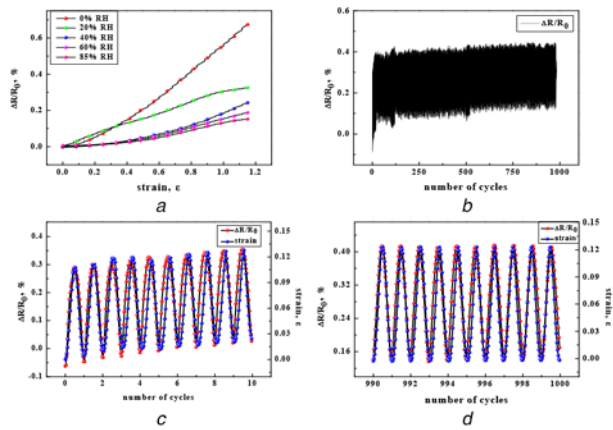


**Fig. 9** Tensile test and fatigue test after relative humidity environment  
*a* Normalised resistance change ( $\Delta R/R_0$ ) increase with strain  
*b* Real-time electrical and mechanical response under cyclic fatigue loading  
*c*, *d* 10, 1000 cycles

processing time progress, it can be explained that the average distance of adjacent nanofillers increase when deionised water penetrates into the conductive network, which results in weakening of the tunnel effect. After a period of time, the water content in the conductive network does not increase with the increase of treatment time. At RH40%, the resistance change of BP first drops and then rises sharply. The reason for this phenomenon may be that the RH is unstable in the early stage, and the temperature in the treatment box keeps increasing. The resistance of the sensor decreases because of the negative temperature effect of CNTs. When the temperature tends to be stable, the negative temperature effect weakened, and the change of resistance is mainly determined by RH. When RH60% treatment is carried out, there is an obvious mutation of the resistance change after about 3200 min of the treatment. It may be due to the constant temperature and humidity treatment of the specimen, the resin inside the material break locally. We carry out tensile and fatigue test in order to verify whether it can continue to be used for health monitoring.

In order to simulate the influence of the humidity environment on the sensor, we have done the related mechanical tests to show whether the sensor has the same applicability as the result of the ATC environment. The relative change of the resistance ( $\Delta R/R_0$ ) for each sample undergoing different range humidity was calculated. It can be seen from Fig. 9*a* that the sensor exhibits excellent characteristics at RH0%. At RH20%, the resistance curve is higher than the blank group at first, and then lower than it, this may be due to the infiltration of a small amount of water equivalent to reinforcing agent, which increases the strength of the material at low strain, with the increase of strain, water is the accelerator of material damage. The tensile property of the sensor is obviously lower than that of RH20% when the RH exceeds 40%. It may be due to the increase of deionised water concentration which leads to the increase of resin damage. When the RH continues to increase, the deionised water contained inside the sensor structure tends to be saturated, which results in the resistance change of BP to stabilise. So, the BP sensors performance tends to stabilise at RH40–RH85%.

In the early stage of fatigue test, The initial resistivity of each cycle increased, because a small amount of deionised water still exists inside the sensor after humidity treatment, which hinders the transmission of electrons between channels during the stretching process. On the other hand, there is the generation of residual resistance. This reason can be verified in Fig. 9*c*. After a period of time, the conductive network of BP is rearranged and stabilised. As can be seen from Figs. 9*c* and *d*, the change of resistance also increases when the applied strain rises, the change of resistance also decreases when the strain reaches the maximum and begins

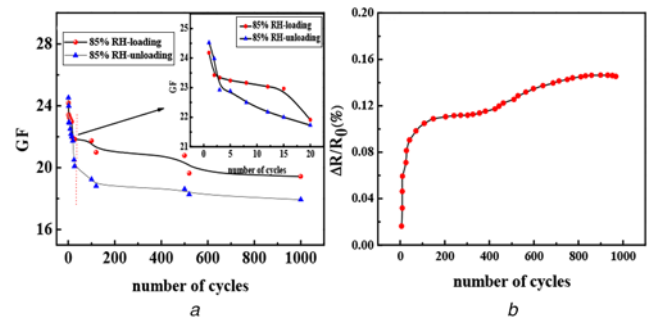


**Fig. 10** Curve of GF and residual resistance after relative humidity  
*a* GF and corresponding cycle  
*b* Residual resistivity change with cycle numbers

to decrease. We can see that there is good coordination between the strain and the change rate of resistance. Therefore, the BP sensors can still be used for health monitoring in the humidity environment of experiment.

In order to verify the above conclusions, we have done a graph of the change of GF with the number of cycles and the change of residual resistivity with the number of cycles. From Fig. 10*a*, it can be seen that the early reduction of GF is more obvious during the loading and unloading process. It tends to be stable after a period of time. The loaded GF is generally higher than unloaded GF. This reason is similar to that of ATC. It is due to the generation of residual resistance and the corresponding strain rate of resistance changes correspondingly during unloading. The same situation can be obtained from Fig. 10*b*. The residual resistivity increases rapidly to about 0.12% in the early stages and then tends to be stable. At around 500 cycles, a small mutation occurs, may due to the local damage of resin matrix caused by the humidity environment, but the overall GF and residual resistivity can be stabilised. In summary, the BP sensors can be applied to the health monitoring of the aviation composite in high temperature and high humidity environment.

**4. Conclusion:** The composite laminates surface bonded with BP sensors were fabricated by a low-cost and sample fabrication processing, BP as a sensor, undergoing temperature and humidity environment, for tensile test and loading–unloading of composite structures was introduced. The following conclusions were obtained: the resistance of the sensor changes significantly in the real-time monitoring of environmental treatment. After the ATC, the performance of the sensor decreases when the strain  $<1.1\%$  in the tensile test, but it still has good linearity. In the fatigue test, the change of sensor resistance and the strain of specimen have a good fit. After the RH, the sensor when the RH  $<40\%$  is changed greatly, and the trend between 40 and 85% slow down, and the sensor is stable after the residual resistance of the resistance in the fatigue test. In the strain sensing coefficient curve, the GF changes larger in the previous dozens of cycles, and then the magnitude of the change decreases. In summary, BP sensors can be applied to SHM of composite materials in complex environments due to its excellent sensing performance, stability and low cost of preparation.

**5. Acknowledgments:** This work was financially supported by the National Nature Science Fund (11602150, U1733123), the Aeronautical Science Foundation (2017ZE54029), the Shenyang Science Project (18-013-0-23), the Natural Science Foundation of Liaoning Province (20170540695) (20180550751), the Scientific Research Fund for Public Welfare of Liaoning province (20170014), the Scientific Research Project of Liaoning Provincial Education Department (L201725). The financial contributions are gratefully acknowledged.

## 6 References

- [1] Iijima S.: 'Helical microtubules of graphitic carbon', *Nature*, 1991, **354**, pp. 56–58
- [2] Hu N., Karube Y., Yan C., *ET AL.*: 'Tunneling effect in a polymer/carbon nanotube nanocomposite strain sensor', *Acta Mater.*, 2008, **56**, pp. 2929–2936
- [3] Wang Z., Liang Z., Wang B., *ET AL.*: 'Kramers processing and property investigation of single-walled carbon nanotube (SWNT) buckypaper/epoxy resin matrix nanocomposites', *Composites Part A*, 2004, **35**, (10), pp. 1225–1232
- [4] Thostenson E.T., Chou T.W.: 'Carbon nanotube networks: sensing of distributed strain and damage for life prediction and self healing', *Adv. Mater.*, 2010, **18**, pp. 2837–2841
- [5] Kunkun W., Zhongsheng L., Haibao L., *ET AL.*: 'Flexible and compressible temperature sensors based on hierarchically buckled carbon nanotube/rubber bi-sheath-core fibers', *J. Nanosci. Nanotechnol.*, 2018, **18**, (4), pp. 2732–2737
- [6] Wichman M.H.G., Buschhorn S.T., Boeger L., *ET AL.*: *Nanotechnology*, 2008, **19**, p. 475
- [7] Yin G., Hu N., Karube Y., *ET AL.*: 'A carbon nanotube/polymer strain sensor with linear and anti-symmetric piezoresistivity', *J. Compos. Mater.*, 2011, **45**, pp. 1315–1323
- [8] Cao C.L., Hu C.G., Fang L., *ET AL.*: 'Humidity sensor based on multi-walled carbon nanotube thin films', *J. Nanomater.*, 2010, **2011**, p. 5
- [9] Baughman R.H., Cui C., Zakhidov A.A., *ET AL.*: 'Carbon nanotube actuators', *Science*, 1999, **284**, pp. 1340–1344
- [10] Rein M.D., Breuer O., Wagner H.D.: 'Sensors and sensitivity: carbon nanotube buckypaper films as strain sensing devices', *Compos. Sci. Technol.*, 2011, **71**, pp. 373–381
- [11] Teague L.C., Banerjee S., Wong S.S., *ET AL.*: 'Effects of ozonolysis and subsequent growth of quantum dots on the electrical properties of freestanding single-walled carbon nanotube films', *Chem. Phys. Lett.*, 2007, **442**, pp. 354–359
- [12] Tao G., Yong Z., Liu W., *ET AL.*: 'Connection of macro-sized double-walled carbon nanotube strands by bandaging with double-walled carbon nanotube films', *Carbon NY*, 2007, **45**, pp. 2235–2240
- [13] Xu G., Qiang Z., Zhou W., *ET AL.*: 'The feasibility of producing MWCNT paper and strong MWCNT film from VACNT array', *Appl. Phys. A*, 2008, **92**, pp. 531–539
- [14] Koratkar N.A., Wei B., Ajayan P.M.: 'Multifunctional structural reinforcement featuring carbon nanotube films', *Compos. Sci. Technol.*, 2003, **63**, pp. 1525–1531
- [15] Koratkar N., Wei B.Q., Ajayan P.M.: 'Carbon nanotube films for damping applications', *Adv. Mater.*, 2010, **14**, pp. 997–1000
- [16] Slobodian P., Lloret Pertegás S., Riha P., *ET AL.*: 'Glass fiber/epoxy composites with integrated layer of carbon nanotubes for deformation detection', *Compos. Sci. Technol.*, 2018, **156**, pp. 61–69
- [17] Ding W., Pengcheng S., Changhong L., *ET AL.*: 'Highly oriented carbon nanotube papers made of aligned carbon nanotubes', *Nanotechnology*, 2008, **19**, p. 075609
- [18] Aly K., Bradford P.D.: 'Real-time impact damage sensing and localization in composites through embedded aligned carbon nanotube sheets', *Compos. B, Eng.*, 2019, **162**, pp. 522–531
- [19] Gou J., Scott O.B., Gu H., *ET AL.*: 'Damping augmentation of nanocomposites using carbon nanofiber paper', *J. Nanomater.*, 2006, **2006**, pp. 7–7
- [20] Luo S., Waris O., Liu T.: 'SWCNT-thin-film-enabled fiber sensors for lifelong structural health monitoring of polymeric composites – from manufacturing to utilization to failure', *Carbon NY*, 2014, **76**, pp. 321–329
- [21] Luo S., Wang Y., Wang G., *ET AL.*: 'CNT enabled co-braided smart fabrics: a new route for non-invasive, highly sensitive & large-area monitoring of composites', *Sci. Rep.*, 2017, **7**, p. 44056
- [22] Wang S., Downes R., Young C., *ET AL.*: 'Carbon fiber/carbon nanotube buckypaper interply hybrid composites: manufacturing process and tensile properties', *Adv. Eng. Mater.*, 2015, **17**, pp. 1442–1453
- [23] Boztepe S., Hao L., Heider D., *ET AL.*: 'Novel carbon nanotube interlaminar film sensors for carbon fiber composites under uniaxial fatigue loading', *Compos. Struct.*, 2018, **189**, p. S0263822317319074
- [24] Koratkar N., Modi A., Lass E., *ET AL.*: 'Temperature effects on resistance of aligned multiwalled carbon nanotube films', *J. Nanosci. Nanotechnol.*, 2004, **4**, (7), pp. 744–748
- [25] Li X., Chen X., Chen X., *ET AL.*: 'High-sensitive humidity sensor based on graphene oxide with evenly dispersed multiwalled carbon nanotubes', *Mater. Chem. Phys.*, 2018, **207**, pp. 135–140
- [26] Bi H., Yin K., Xie X., *ET AL.*: 'Ultrahigh humidity sensitivity of graphene oxide', *Sci. Rep.*, 2013, **3**, p. 2714
- [27] Trulli M.G., Sardella E., Palumbo F., *ET AL.*: 'Towards highly stable aqueous dispersions of multi-walled carbon nanotubes: the effect of oxygen plasma functionalization', *J. Colloid Interface Sci.*, 2017, **491**, pp. 255–264
- [28] Adjizian J.J., Leghrib R., Koos A.A., *ET AL.*: 'Boron- and nitrogen-doped multi-wall carbon nanotubes for gas detection', *Carbon NY*, 2014, **66**, pp. 662–673
- [29] Memon M.O., Haillot S., Lafdi K.: 'Carbon nanofiber based buckypaper used as a thermal interface material', *Carbon NY*, 2011, **49**, (12), pp. 3820–3828
- [30] Gao J., Loo Y.-L.: 'Temperature-Dependent Electrical Transport in Polymer-Sorted Semiconducting Carbon Nanotube Networks', *Adv. Funct. Mater.*, 2015, **25**, (1), pp. 105–110
- [31] Shaowei L.U., Feng C., Nie P., *ET AL.*: 'Fabrication of carbon nanotube buckypaper by spray-vacuum filtration method and its strain and temperature sensing properties', *Acta Aeronaut. Et Astronaut. Sin.*, 2015, **36**, (09), pp. 3187–3194
- [32] Yoo K.P., Lim L.T., Min N.K., *ET AL.*: 'Novel resistive-type humidity sensor based on multiwall carbon nanotube/polyimide composite films', *Sens. Actuators B Chem.*, 2010, **145**, pp. 120–125